Adsorption and reaction of water on the AlN(0001) surface from first principles

Chen, Yafeng; Hou, Xinmei; Fang, Zhi; Wang, Enhui; Chen, Junhong; Bei, Guoping

DOI
10.1021/acs.jpcc.8b11228

Publication date
2019

Document Version
Final published version

Published in
Journal of Physical Chemistry C

THE JOURNAL OF PHYSICAL CHEMISTRY C

Article

Cite This: J. Phys. Chem. C 2019, 123, 5460−5468

pubs.acs.org/JPCC

Adsorption and Reaction of Water on the AlN(0001) Surface from First Principles

Yafeng Chen,[†] Xinmei Hou,*[,†] Zhi Fang,[†] Enhui Wang,[†] Junhong Chen,[‡] and Guoping Bei[§]

[†]Collaborative Innovation Center of Steel Technology and [‡]School of Materials Science and Engineering, University of Science and Technology Beijing, Beijing 100083, China

[§]Department of Materials Science and Engineering, 3ME, Delft University of Technology, Mekelweg 2, 2628CD Delft, The Netherlands

Supporting Information

ABSTRACT: Aluminum nitride (AlN) with a combination of very high thermal conductivity and excellent electrical insulation properties exhibits wide applications. However, it is quite sensitive to a moist environment and hydrolyzes slowly in water. In this work, density functional theory was adopted to examine the atomistic reaction mechanism on the wurtzite AlN(0001) surface. The results indicate that water molecules are preferentially adsorbed at the top site of the AlN(0001) surface. The decomposition of adsorbed H_2O into OH and H on the AlN(0001) surface occurs spontaneously without any energy barrier. However, a further dissociation reaction of OH into O and H has an energy barrier of 22.046 kcal/mol. The dissociation of H_2O is strongly dependent on the H_2O coverage when more water molecules are adsorbed. Ammonia (NH_3) is determined as the dominant gas product at 4/9 monolayer H_2O coverage, which will induce N vacancy (V_N) formation in AlN ceramic. The V_N will be occupied by O^{2-} after geometry optimization and plays an acceleration role in the degradation of AlN by water. H_2O adsorption and the formation of NH_3 occur alternately with the H_2O coverage increasing. An OH−Al−O layer is formed as a precursor of AlOOH after the first AlN bilayer is fully degraded. This work can guide the manufacture and application of AlN from the theoretical viewpoint.

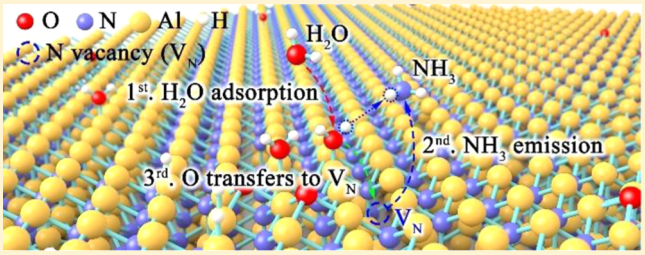

1. INTRODUCTION

Aluminum nitride (AlN) has attracted significant attention because of its low thermal expansion coefficient ($(4.03-6.0) \times 10^{-6}$ K^{-1}) near to that of silicon, a wide band gap (6.2 eV), excellent thermal conductivity (3.2 W/(cm K)), high chemical stability, high electrical resistivity ($>4 \times 10^8$ Ω cm), and good mechanical properties at high temperatures.[1−3] Therefore, it is widely applied as structural ceramics,[4,5] sintering additives,[6,7] semiconductor devices,[8] optoelectronic and field emission devices,[9] and so on. However, the propensity for AlN to hydrolyze and generate ammonia precludes the use of water during the manufacturing process of AlN substrates, which increases the cost and complexity of the process.[10] Besides, AlN must be processed under strict conditions to avoid oxidation via hydrolysis because oxygen impurities in AlN have been identified as the primary cause of reducing its remarkable properties.[11,12]

To understand the reaction mechanisms between water and AlN, a few experimental studies have been carried out.[13−17] Li et al.[14] investigated the mechanism and kinetics of AlN powder degradation in moist air at room temperature. They proposed three reaction stages during the degradation. The first stage was an induction period, during which the surface aluminum oxide or oxyhydroxide layer was formed slowly. In the second stage, fast hydrolysis occurred that was correlated to the chemical reaction rate dealing with the unreacted-core model. Finally, gradual closure of pores in the structure of $Al(OH)_3$ around AlN was observed. In this stage, the hydrolysis rate was also lower and mainly controlled by mass transfer through $Al(OH)_3$ around the unreacted AlN ceramic. Kocjan et al.[13] found that the starting temperature and the ageing time for hydrolysis of AlN powders had an impact on the reaction products and their morphologies. At room temperature, the main crystalline reaction product was bayerite ($Al(OH)_3$) regardless of the ageing time in the mother liquor. However, at higher temperatures, the hydrolysates varied with the temperature and ageing time. Boehmite (AlOOH) was detected as the initial hydrolysis product. With ageing time increasing, both AlOOH and $Al(OH)_3$ appeared. With aging time prolonging up to 24 h, $Al(OH)_3$ was detected as the predominate phase in the 40−70 °C temperature range. AlOOH became the predominated product with the temperature further increasing up to 80−90 °C. Besides above work, some theoretical studies[18,19] have been reported to explore the effect of water adsorption on the AlN nanocones and nanotubes. Bartel et al.[10] investigated the reaction mechanisms of the initial stages

Received: November 21, 2018
Revised: January 29, 2019
Published: February 14, 2019

DOI: 10.1021/acs.jpcc.8b11228
J. Phys. Chem. C 2019, 123, 5460−5468

of AlN hydrolysis using density functional theory (DFT). The process involves water adsorption, hydroxyl-mediated proton diffusion to form NH_3, and NH_3 desorption. It was found that hydroxyl-mediated proton diffusion is the predominant mechanism in AlN hydrolysis.

In this work, the reaction behavior between AlN and water is fundamentally investigated at the atomistic level using DFT, aiming to provide an insight into the understanding of hydrolysis of AlN. Since (0001) and $(000\bar{1})$ polar are the most common surfaces of wurtzite AlN and the (0001) surface owns the lowest density of surface energy,[20−23] the H_2O molecule on the AlN(0001) clean surface with lower adsorption energy is concerned in this work.

2. COMPUTATIONAL DETAILS

First principles calculations are performed using the plane-wave pseudopotential implementation of DFT as written in the CASTEP code.[24] The exchange−correlation function is approximated by the generalized gradient approximation and the Perdew−Burke−Ernzerhof (GGA-PBE)[25] that is essential to achieve a good description of hydrogen bonds.[26,27] The Tkatchenko and Scheffler[28] (TS) corrections to the PBE are adopted to correct DFT for missing van der Waals interactions and the interaction between the H_2O molecules. The ionic cores are described by ultrasoft pseudopotentials[29] to improve transferability and reduce the number of plane waves required in the expansion of the Kohn−Sham orbitals.

The AlN(0001) surface is modeled by a slab geometry including a 15 Å vacuum region and periodically repeated in the direction perpendicular to the surface. The slab supercell consists of 3 × 3 AlN unit cells with six AlN bilayers (Figure 1). Among these layers, the bottom four AlN layers are fixed at

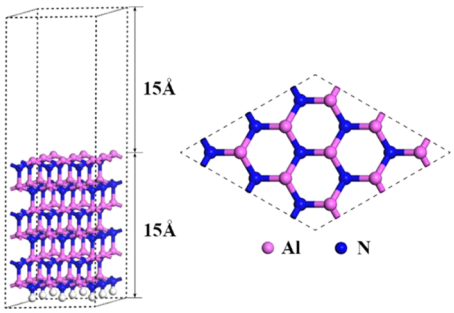

Figure 1. Configuration of the AlN(0001) slab model and its top view.

the ideal position to simulate a bulk environment. The other atoms in the first two AlN bilayers of the slab are relaxed until the residual force is smaller than 0.03 eV/Å after implementing structural optimization. To avoid the artificial charge transfer and decouple the two surfaces of the slab, the pseudohydrogens with fractional charges are deposited on the N/Al-terminated bottom side of the slab (the N−H bond distances have been optimized).[30] The Brillouin zone integral is evaluated according to the Monkhorst−Pack *k*-point sampling scheme[31] with the tetrahedron method and Blöchl correction.[32] A 3 × 3 × 1 *k*-point mesh through the convergence test is adopted in all of the calculations to ensure sufficient accuracy of the interfacial energies. The cutoff energy of 400 eV is chosen through the convergence test, which is enough for the energy calculation to get convergence including AlN clean surface structures and molecule adsorption structures (Figure S1). At this cutoff energy and *k*-point density, the short lattice constant obtained for the wurtzite AlN is a = 3.110 Å and the c/a ratio is 1.60. This is in good agreement with the experimental data, i.e., a = 3.111 Å and c/a ratio 1.60.[33]

3. RESULTS AND DISCUSSION

3.1. H_2O Adsorption and Dissociation on the Clean AlN(0001) Surface. H_2O is adsorbed on the upper surface of the AlN slab. All adsorption energies are extracted from a fully relaxed structure. The adsorption energy for H_2O on the AlN(0001) surface, E_i^{ads}, is defined as follows

$$E_i^{ads} = E_{i-1}^{total} + \mu_{H_2O} - E_i^{total} \quad (1)$$

where i is the number of water molecules and E_i^{total} and E_{i-1}^{total} are the total energies of the optimized structures with i and $i-1$ water molecules, respectively. μ_{H_2O} is the chemical potential calculated from the total energy of a single H_2O molecule. According to eq 1, the more positive the adsorption energy values, the stronger the interactions between H_2O and the AlN surface and thus the more stable the adsorption structure.

Considering H_2O adsorption, there are four different adsorption orientations at the four sites (top, bridge, face-centered cubic (fcc), and hexagonal close-packed (hcp), marked in Figure 2a). If the four different adsorption

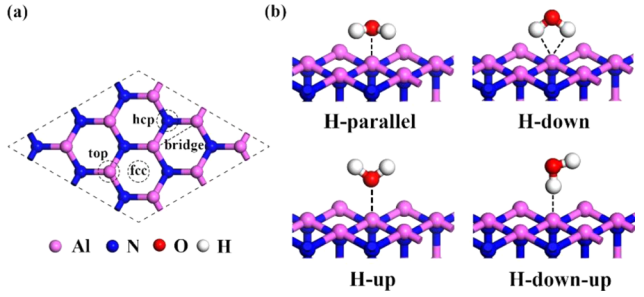

Figure 2. (a) Initial adsorption sites on the AlN(0001) surface. (b) Four different adsorption orientations: H-parallel, the H_2O molecule plane is parallel to the AlN surface; H-down, he H_2O molecule plane is normal to the AlN surface with two hydrogen atoms sitting at the same height and two hydrogen atoms below the oxygen atom; H-up, the H_2O molecule plane is normal to the AlN surface with two hydrogen atoms sitting at the same height and above the oxygen atom; and H-down-up, the H_2O molecule plane is normal to the AlN surface with only one O−H bond pointing to the AlN surface.

orientations in the initial structures are represented as H-parallel, H-up, H-down, H-down-up, and H-parallel, respectively, as shown in Figure 2b, there are 16 different initial adsorption configurations of H_2O on the AlN surface (Figure S2a). The optimized structures are shown in Figure S2b. The average bond lengths (d), the angles between some atoms and planes ($\angle$), and the adsorption energies (E_{ads}) are summarized in Table 1. Based on the calculation results, two distinct adsorption features of H_2O on the AlN(0001) surface can exist, corresponding to molecular adsorption and H−OH dissociative adsorption. For these molecular adsorption structures, they can be divided into two categories on the basis of the orientation of the H−O−H angle. As for these H−OH dissociative adsorption structures, they can also be divided into two categories according to the adsorption site of OH species. According to the key structural parameters and adsorption energies, four stable adsorption configurations

DOI: 10.1021/acs.jpcc.8b11228
J. Phys. Chem. C 2019, 123, 5460−5468

Table 1. Key Structural Parameters and Adsorption Energies for Sixteen Stable Structures of H_2O on the AlN(0001) Surface

	d_{Al-O} (Å)	d_{Al-H} (Å)	d_{O-H} (Å)	∠Al−O−H (deg)	∠H−O−H (deg)	E_{ads} (eV)
top H-parallel	1.92		1.01	110.50	109.74	1.3196
top H-down	1.91		1.01	109.96	110.56	1.3047
top H-up	1.91		1.02	110.15	110.88	1.3392
top H-down-up	1.91		1.00	114.12	111.67	1.2897
fcc H-parallel	1.91		1.01	110.7	109.28	1.3177
fcc H-down	1.91		1.01	112.56	109.59	1.3294
fcc H-up	1.96	1.61	0.98			3.3184
fcc H-down-up	1.91		1.02	114.38	110.14	1.287
hcp H-parallel	1.73	1.6	0.97	126.6		3.1923
hcp H-down	1.79		1.13	115.83	110.67	1.2892
hcp H-up	1.96	1.61	0.98	131.7		3.502
hcp H-down-up	1.73	1.6	0.97	126.24		3.2399
bridge H-parallel	2.05	1.64	0.91	119.72		3.2327
bridge H-down	1.92		1.01	110.5	110.09	1.3275
bridge H-up	2.08	1.61	0.98			3.459
bridge H-down-up	1.92		1.01	110.16	109.38	1.352

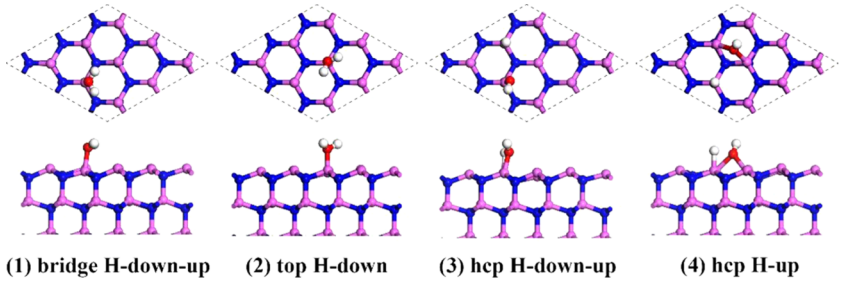

Figure 3. Four stable initial adsorption configurations of H_2O on the AlN(0001) surface. (1) Bridge site with H-down-up orientation; (2) top site with H-down orientation; (3) hcp site with H-down-up orientation; and (4) hcp site with H-up orientation.

corresponding to the above four kinds of adsorption features are selected and shown in Figure 3.

The two stable molecule adsorption structures for H_2O on the AlN(0001) surface are shown in Figure 3(1),(2), which have the near adsorption energies (1.3520 and 1.3047 eV) and similar adsorption structural parameters. In both structures, H_2O prefers to adsorb at the top site with the parallel mode. The angles between the H_2O molecule plane and the AlN(0001) surface are 111.16 and 109.96°, respectively. The adsorbed H_2O molecules are still in C_{2v} symmetry with the O−H distance of 1.01 Å and the H−O−H angle of 109.74°, as shown in Table 1. The only difference between the structures of Figure 3(1),(2) is the orientation of the H−O−H angle. The H−O−H angle in Figure 3(1) is toward the fcc site, whereas it is toward the hcp site in Figure 3(2). The H_2O molecule can be dissociated into adsorbed OH and H species on the AlN(0001) surface, as shown in Figure 3(3),(4). As shown in Figure 3(3), the OH and H species prefer to adsorb at the top sites with a 3.2399 eV adsorption energy. The bond lengths of formed Al−H and Al−O bonds are 1.60 and 1.73 Å, respectively. Besides this, the H atom can be adsorbed at the top site, whereas the OH species prefer to locate at the bridge site, bonding with two surface Al atoms through an O atom with a 1.96 Å bond length as shown in Figure 3(4). The adsorption energy is 3.502 eV, more positive than that of Figure 3(3), revealing that it is a more stable structure of H−OH dissociative adsorption. Considering that H_2O adsorbs dissociatively on the AlN(0001) surface, the energy barriers for H_2O molecule dissociation are computed. The dissociation pathways and optimized structures for H_2O on the AlN(0001) surface are summarized in Figure 4. It indicates that the decomposition of adsorbed H_2O into OH and H on the AlN(0001) surface occurs spontaneously without any energy barrier. However, for a further dissociation reaction of OH into O and H, it has an energy barrier of 22.046 kcal/mol with a reaction heat close to −41.68 kcal/mol. The low activation energy and high release exothermicity indicate that the further dissociation reaction can proceed at room temperature. Therefore, the adsorption energies for molecular adsorption (H_2O), partially dissociative adsorption ($H_2O \rightarrow OH + H$), and completely dissociative adsorption ($H_2O \rightarrow O + 2H$) with different initial adsorption configurations are calculated. The

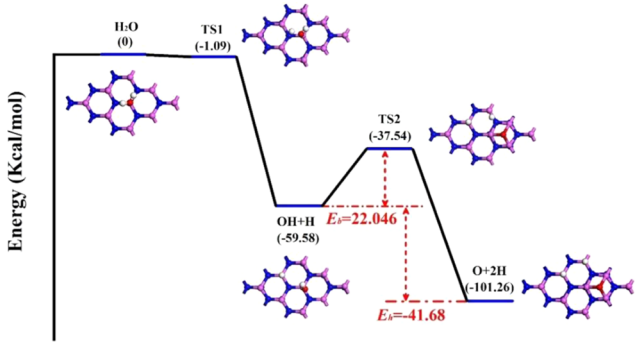

Figure 4. Dissociation pathways and optimized structures of H_2O on the AlN(0001) surface. E_b and E_h are the energy barrier and the reaction heat of the further dissociation reaction of OH into O and H, respectively.

DOI: 10.1021/acs.jpcc.8b11228
J. Phys. Chem. C 2019, 123, 5460−5468

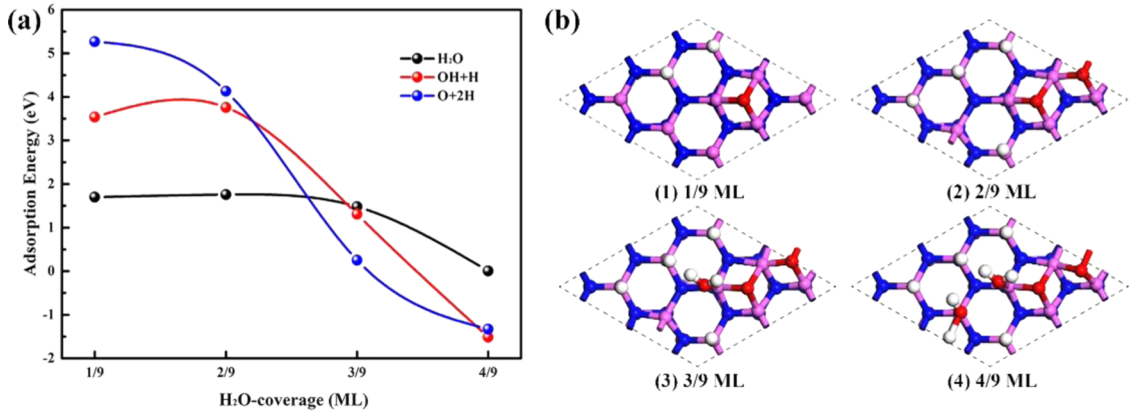

Figure 5. (a) Relationship between adsorption energy and H_2O coverage. (b) Most stable structures at different H_2O coverages.

most stable structures of three different initial adsorption configurations are shown in Figure S3. It has been found that the completely dissociative adsorption ($H_2O \rightarrow O + 2H$) owns the lowest adsorption energy. In this structure, the H atoms are located at the top site and the O atom at the fcc site bonding with surface Al atoms.

Since the number of the top sites at the 3 × 3 AlN surface structure is nine, the H_2O coverage can be expressed as 1/9, 2/9,..., 8/9, 1 monolayer (ML). The H_2O adsorption energy and structures on the AlN(0001) surface as a function of H_2O coverage are revealed in Figure 5. Concerning the H_2O coverage at 1/9 and 2/9 ML, the completely dissociative adsorption of the water molecule has the highest adsorption energy (Figure 5a), which indicates that at these two H_2O coverages the completely dissociative adsorption structures (Figure 5b(1),(2)) are the most stable structures. However, for the H_2O coverage at 3/9 and 4/9 ML, molecular adsorption owns the highest adsorption energy (Figure 5a). It may be attributed to the increasing interaction force among the adsorbed OH, O, and H species with the increase of H_2O coverage. Thus, the water molecular adsorption structure (Figure 5b(3),(4)) will be considered as the most stable. Considering H can easily interact with adjacent OH to form H_2O after geometry optimization at the higher H_2O coverage, the adsorption of the water molecule tends to be completely dissociative adsorption at low H_2O coverage (≤2/9 ML) and then transforms into molecular adsorption at high H_2O coverage (>2/9 ML). Therefore, the dissociative adsorption is no longer taken into consideration in the following calculations.

3.2. Gaseous Product Formation. To confirm the gaseous products, the formation energies of possible gaseous products, e.g., NO_2, NO, N_2, H_2, or NH_3[15,23,34,35] at different H_2O coverages were calculated on the basis of the following equation

$$E_{form} = E^{total}_{surface} - E^{total}_{surface\text{-}gas} - \mu_{gas} \quad (2)$$

where E_{form} represents the formation energy of gas (NO_2, NO, N_2, H_2, or NH_3) and $E^{total}_{surface}$ and $E^{total}_{surface\text{-}gas}$ are the total energies of the H_2O-adsorbed AlN(0001) surfaces before and after gas emission of NO_2, NO, N_2, H_2, or NH_3, respectively. μ_{gas} is the chemical potential of the gas product. In this work, we just assume that the gas products are desorbed and separated from the AlN surface. Therefore, the calculation focuses on the initial and final states of the AlN surface. The intermediate states of gas absorption on the AlN surface are not taken into consideration.

As demonstrated in Figure 6, the formation energies for NO_2, NO, and N_2 are always negative, indicating that the

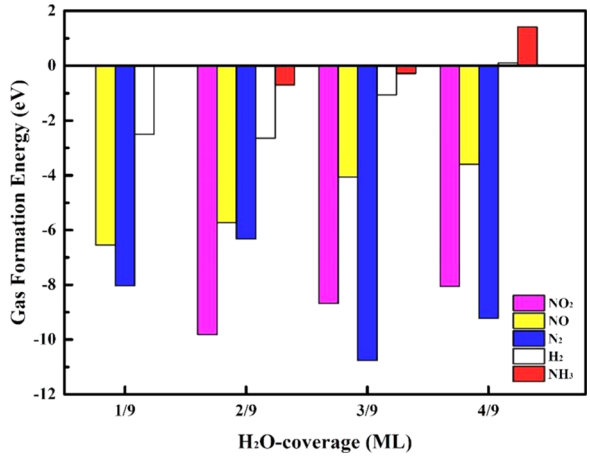

Figure 6. Formation energies of gas products (NO_2, NO, N_2, H_2, and NH_3) at 1/9, 2/9, 3/9, and 4/9 ML H_2O coverages.

structures with nitrogen oxides or nitrogen gas are thermodynamically unstable. As for the formation of H_2, although the formation energy turns positive at 4/9 ML coverage, the value is very small (0.1021 eV). In addition, assuming H_2 would be produced, the valence state of H should change from +1 to 0. From the viewpoint of electronegativity, the electron is obtained relatively easier from N^{3-} than O^{2-}.[36] If electrons transfer from N^{3-} to H^+, NO, NO_2, or N_2 would be formed along with the simultaneous formation of H_2, which is inconsistent with above calculations. Thus, the further dehydrogenation of the adsorbed water molecule to form H_2 is impossible but may occur at relatively high temperatures.[37] Besides H_2, the formation energy of NH_3 became positive with increasing H_2O coverage, i.e., 1.4127 eV at 4/9 ML H_2O coverage, indicating that NH_3 will be the dominant gas product. From the structural analysis (shown in Figure S4), one of N^{3-} on the AlN(0001) surface would be removed with the formation of NH_3 to form N vacancies (V_N) in these structures. Owing to the existence of V_N, the energies of the AlN surface structures become higher, which leads to the formation energies of gas products turn negative. Therefore, the surface structures with V_N existence are unstable. To

DOI: 10.1021/acs.jpcc.8b11228
J. Phys. Chem. C 2019, 123, 5460−5468

reduce the total energy of the surface, the V_N sites will be occupied by O^{2-} spontaneously after geometry optimization at 4/9 ML H_2O coverage. As a result, the formation energy of NH_3 turns to positive. Figure 7 shows the structure with an

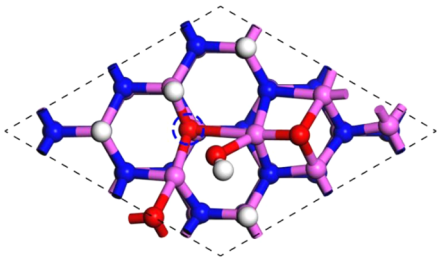

Figure 7. Most stable structure with an O^{2-} atom migrating to the V_N site labeled by a dashed blue circle after NH_3 removal.

O^{2-} atom migrating to the V_N site after the removal of NH_3. It can be seen that with the occupation of O^{2-} at the V_N site NH_3 emission occurs and the structure becomes stable. This is also in good agreement with the results reported in the literature.[15,38]

3.3. Electronic Structure Variation during AlN(0001) Surface Hydrolysis. The change in material properties always originates from electronic structure variation. To better understand the innermost physics of O^{2-} migration, densities of states for some surface structures were calculated (Figure 8). The results indicate that the peak in the dashed red rectangle located at 2.66 eV (Figure 8a) is mainly attributed to Al 3s and 3p state electrons around the V_N site (Figure 8b). The Al atoms around this V_N site generate more dangling bonds because of the presence of V_N and the breaking of Al−N bonds. These dangling bonds of Al atoms cause the formation of surface states near the conduction band minimum according to Miao's report.[39] When N^{3-} is removed in the form of NH_3, the valence state of N is kept as −3. Thus, the share electron pairs in the Al−N bond split from Al^{3+} by NH_3, causing three new unoccupied molecular orbitals (UMOs) of Al to form the Al surface states (Figure 8a). It is widely accepted that surface states play an important role in the charge transfer and surface reconstruction.[40] With the existence of surface states, there is an electric field on the surface that may affect some surface properties.[41] Electrons, especially the lone-pair electrons around these UMOs, trend to transfer and being occupied by the driving of electronic field, leading to the charge transfer and electron density redistribution. Besides the movement of electrons, some atoms or ions can also migrate to a more stable site, leading to surface reconstruction. Among the atoms or ions around UMOs, O^{2-} with p lone-pair electrons has a top priority to move to the place where the p lone-pair electrons can occupy the UMOs. The V_N site is exactly the perfect place for O^{2-} via consuming the O p lone-pair electrons and passivating the dangling bond states of Al. The UMOs are occupied to form occupied molecular orbitals and thus is shifted down to valence band minimum. Hence, Al surface states disappear after passivation (Figure 8a,c). The O 2p and Al 3s, 3p orbits in the green dashed rectangle (Figure 8d) exhibit apparent resonance, showing the strong hybridization between them and the formation of Al−O bonds. The energy of the AlN surface decreases with the formation of Al−O bonds.

To further understand the charge transfer and redistribution of charge density during the migration of O^{2-} to the V_N site, the difference charge density map was calculated. Figure 9 shows the difference electron density of the stable structures with the V_N site and with V_N occupied by O^{2-}, respectively. The isosurface of difference charge density is plotted at a value of about 0.1 e/Å^3. The blue and yellow isosurfaces represent

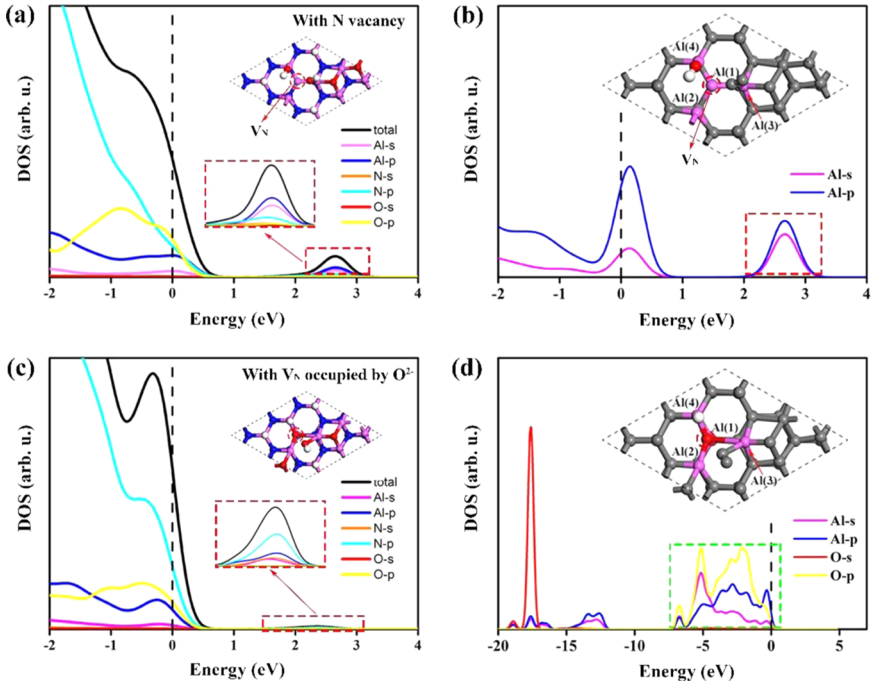

Figure 8. (a) Total and partial density of states for the AlN surface with N vacancy. (b) Partial density of states for the four Al atoms around the V_N site. (c) Total and partial density of states for the AlN surface with the V_N occupied by O^{2-}. (d) Partial density of states for the four Al atoms around the V_N site and the O^{2-} occupied in the V_N site.

DOI: 10.1021/acs.jpcc.8b11228
J. Phys. Chem. C 2019, 123, 5460−5468

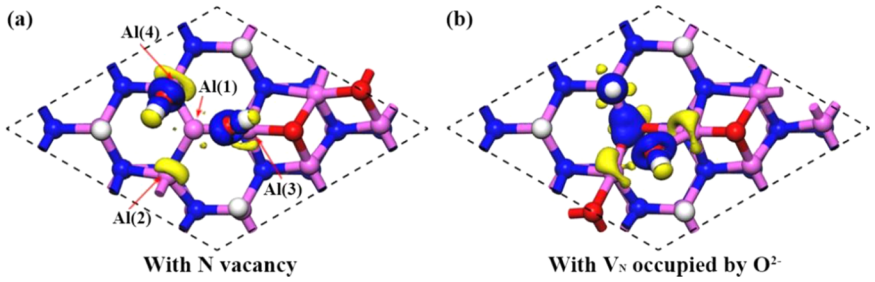

Figure 9. Difference charge density of the stable structures with the V_N site and with V_N occupied by O^{2-}. (Isosurfaces of the difference charge density with blue and yellow isosurfaces indicating charge accumulation and charge depletion regions, respectively).

the charge accumulation and depletion regions, respectively. To distinguish different Al atoms, the four Al atoms around the V_N are named as Al(1), Al(2), Al(3), and Al(4), labeled in Figure 9a. It can be seen that there is a large charge redistribution around the V_N site by comparing Figure 9a,b. For the surface structure with the V_N site occupied by O^{2-}, there is a large region of charge accumulation around the V_N site. In addition, a distinct region of electron depletion around the Al atoms that are close to the V_N site can be observed. This indicates the strong hybridization of O and Al atomic orbitals, which is attributed to the formation of Al−O bonds.[42] For the O^{2-} connecting with Al(3) in Figure 9a, it migrates to the bridge site. The charge redistribution around it indicates that this O^{2-} forms another Al−O bond with Al(2), which makes the structure more stable.

The Mulliken charges of some atoms around the V_N site are summarized in Table 2 that can analyze the charge transfer quantitively.[43] Before the O^{2-} migrates to the V_N site, it was only bonded with the Al(4) atom and the H atom. Due to a low electronegativity of Al atom, the charge of Al(4) atom is positive. Al(1), Al(2), and Al(3) generate dangling bonds with the existence of the V_N site. After the V_N site is occupied by O^{2-}, the O^{2-} bonds with another three Al atoms and causes the positive charge of Al(4) to decrease. This change is the same as with the electron density transformation around Al(4) atom (Figure 9). With the V_N site being occupied by O^{2-}, the positive charge of Al(1), Al(2), and Al(3) atoms increases, which agrees with the charge depletion around the three Al atoms by comparing Figure 9a,b. This result verifies that electrons transfer from Al atoms to the O atom during the migration process. This can be attributed to the formation of Al−O bonds and the high electronegativity of the O atom. From the above calculation, it can be concluded that V_N plays an acceleration role in the degradation of AlN by water. O^{2-} of H_2O prefers to occupy the V_N site via consuming the O p lone-pair electrons and UMOs of Al.

Table 2. Mulliken Charge of Some Atoms around the V_N Site

atom	s	pp	total	charge (*e*)	note
Al(1)	0.80	1.32	2.12	0.88	with N vacancy
	0.57	0.96	1.53	1.47	with V_N occupied by O^{2-}
Al(2)	0.78	1.01	1.79	1.21	with N vacancy
	0.59	0.82	1.41	1.59	with V_N occupied by O^{2-}
Al(3)	0.64	0.96	1.59	1.41	with N vacancy
	0.58	0.78	1.36	1.64	with V_N occupied by O^{2-}
Al(4)	0.60	0.98	1.58	1.42	with N vacancy
	0.73	1.04	1.77	1.23	with V_N occupied by O^{2-}
O	1.84	5.27	7.1 2	−1.12	with N vacancy
	1.86	5.23	7.09	−1.09	with V_N occupied by O^{2-}

3.4. Stepwise Reactions. Numerous adsorption structures at different sites with the increase of water molecule coverage are further computed step by step to investigate the adsorption and reaction processes of H_2O on the AlN(0001) surface. In each step, two possible circumstances are concerned, one is the adsorption of H_2O (the sign of "+H_2O") and another is the removal of NH_3 (the sign of "−NH_3"). The reaction energy of step *i* is defined as

$$E_i^{H_2O} = E_{i-1}^{total} + \mu_{H_2O} - E_i^{total} \quad (3)$$

or

$$E_i^{NH_3} = E_{i-1}^{total} - E_i^{total} - \mu_{NH_3} \quad (4)$$

where E_i^{total} and E_{i-1}^{total} are the total energies of the optimized structures in steps *i* and $i-1$, respectively. μ_{H_2O} and μ_{NH_3} are the chemical potentials of a H_2O and a NH_3 molecule, respectively. Equations 3 and 4 are employed to calculate the reaction of H_2O adsorption and NH_3 removal, respectively. Figure 10 demonstrates the free energy evolution and configurations of products for each step after calculating all of the possible reactions in each step. The free energy and its difference between steps *i* and $i-1$ are adopted to exhibit the free energy evolution and the dominated reaction path, which is plotted in Figure 10a. The green ball stands for the initial free energy of the AlN(0001) surface. The red line means the most possible reaction progress and the red ball is corresponding to the structure in Figure 10b for each step. There are many dangling bonds on the Al/N-terminated (0001) surface, and each Al dangling bond contributes 3/4 electrons. Therefore, in the first two steps, H_2O tends to be adsorbed in the form of O and H species on the AlN(0001) surface (Figure 10b(1),(2)) to passivate the dangling bonds states. In steps 3 and 4, the molecular adsorption of H_2O takes place (Figure 10b(3),(4)). In step 5, when H_2O coverage is 4/9 ML, one N atom will be removed while bonding with three H atoms to form a NH_3 molecule. An O^{2-} will occupy the V_N site spontaneously to decrease the AlN surface energy (Figure 10b(5)). In steps 6 and 7, the adsorption of H_2O is preferential than NH_3 removal reaction (Figure 10b(6),(7)). In step 8, the second NH_3 molecule formed when the H_2O coverage is 6/9 ML (Figure 10b(8)). Similarly, in the following steps (Figure 10b(9)−(12)), it is going to absorb two H_2O molecules and then generate an NH_3 molecule. From the above result, the adsorption sites for H_2O absorbed on the AlN(0001) surface are limited. With the H_2O coverage increasing, it becomes difficult to adsorb more H_2O molecules. However, with the spontaneous generation of NH_3 gas and the migration of O^{2-},

DOI: 10.1021/acs.jpcc.8b11228
J. Phys. Chem. C 2019, 123, 5460−5468

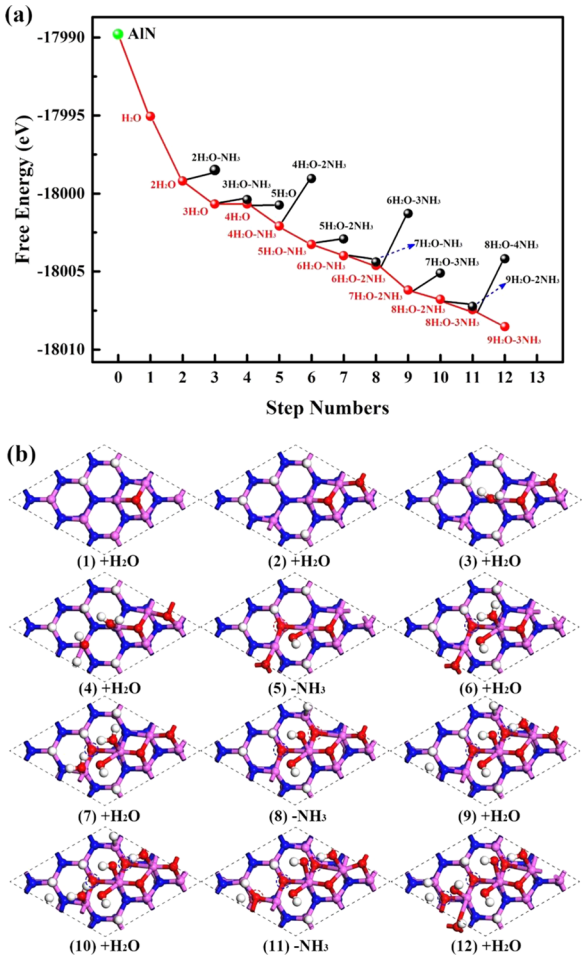

Figure 10. (a) Reaction processes and the energy evolution of each step (the green ball means the initial energy of the AlN(0001) surface that is normalized to zero). The red line means the most possible reaction progress. (b) Optimized structures of the stepwise processes. The sign $+H_2O$ means a H_2O molecule adsorbed in this reaction step, and the sign $-NH_3$ means removing a N atom in the form of NH_3 gas, with the V_N site occupied by O^{2-}.

the adsorption sites are released leading to more H_2O molecules absorption and further reaction with the AlN surface. Thus, the AlN surface will be continuously consumed by water.

Based on above DFT calculations, the final structure of AlN exposed to water is also investigated. The structures (Figure 10b) show that the hydroxy groups tend to occupy the fcc sites and the N atoms are replaced by O atoms. In an analogous way, an ideal model of the final structure with all N atoms replaced by O atoms at the first AlN bilayer is proposed. Its top and side views shown in Figure 11 indicate that each hydroxy group bonds with three aluminum atoms. At the same time, each aluminum atom bonds with three hydroxy groups. The first bilayer can be regarded as a kind of aluminum monohydroxide in molecule composition, and the structure is similar to a precursor of AlOOH. With the coverage of water molecules increasing, the interatomic action force will become stronger and the lattice of this first bilayer structure will be destroyed. The AlOOH can evolve into other aluminum hydroxides, such as bayerite, nordstrandite, and gibbsite, by reacting with H_2O.[13,38]

4. CONCLUSIONS

In summary, adsorption of multiple water molecules and their reaction on the AlN(0001) surface have been investigated based on DFT calculations. The calculation results from many different adsorption configurations of H_2O on the AlN surface reveal that H_2O can be adsorbed on the clean AlN(0001) surface by both molecular adsorption and dissociative adsorption styles depending on the H_2O coverage. The decomposition of adsorbed H_2O into OH and H on the AlN(0001) surface occurs spontaneously without any energy barrier, but a further dissociation reaction of OH into O and H has an energy barrier of 22.046 kcal/mol. Water molecules tend to be completely dissociated and adsorbed in the form of O and H species at a low H_2O coverage ($\leq$2/9 ML) on the AlN(0001) surface, whereas they prefer to be molecular adsorption structures at a high H_2O coverage (>2/9 ML). NH_3 is verified to be the dominant gas product and will be generated when the H_2O coverage is above 4/9 ML. When a N atom from the first bilayer is removed, the N atom will be bonded with three H atoms to form an NH_3 molecule. After NH_3 emission, a V_N will be formed and O^{2-} of H_2O prefers to occupy the V_N site via consuming the O p lone-pair electrons and unoccupied molecular orbital of Al. V_N can accelerate the degradation of AlN by water. The stepwise processes of adsorption of more water molecules and their reaction on the AlN(0001) surface reveal that H_2O adsorption and NH_3 emission occur alternately until all N^{3-} of the first AlN bilayer are replaced. When the first bilayer of AlN is fully degraded, all N^{3-} are replaced by O^{2-} and each hydroxy group is located at the fcc site bonding with three Al atoms. An OH−Al−O layer, a precursor of AlOOH, is formed. With the H_2O coverage increasing, the structure of AlOOH will be destroyed to form other aluminum hydroxides by reacting with H_2O.

■ ASSOCIATED CONTENT

Supporting Information

The Supporting Information is available free of charge on the ACS Publications website at DOI: 10.1021/acs.jpcc.8b11228.

Convergence test of a stable molecule adsorption structure (Figure S1), 16 different initial adsorption

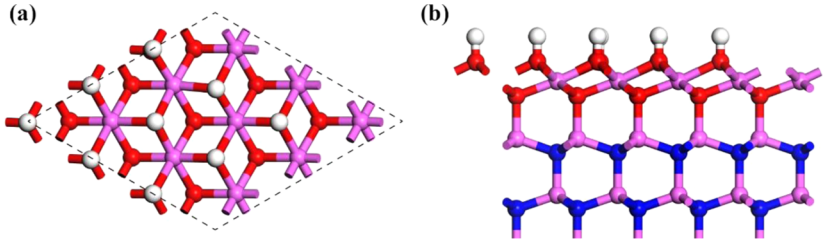

Figure 11. Top (a) and side (b) views of the ideal final structure model with all N atoms replaced at the first AlN bilayer.

DOI: 10.1021/acs.jpcc.8b11228
J. Phys. Chem. C 2019, 123, 5460−5468

configurations of H_2O on the AlN surface and the optimized structures at different sites with different adsorption orientations (Figure S2), three most stable initial structures of H_2O on the AlN(0001) surface (Figure S3), and optimized structures with different gas products removed at different H_2O coverages (Figure S4) (PDF)

AUTHOR INFORMATION

Corresponding Author

*E-mail: houxinmeiustb@ustb.edu.cn. Tel/Fax: +86 010 6233 2570.

ORCID

Xinmei Hou: 0000-0001-9486-478X

Notes

The authors declare no competing financial interest.

ACKNOWLEDGMENTS

The authors express their appreciation to the National Natural Science Foundation for Excellent Young Scholars of China (no. 51522402). The authors also appreciate the Fundamental Research Funds for the Central Universities (FRF-TP-15-006C1) for financial support.

REFERENCES

(1) Wu, H. M.; Peng, Y. W. Investigation of The Growth and Properties of Single-Crystalline Aluminum Nitride Nanowires. *Ceram. Int.* **2015**, *41*, 4847−4851.

(2) Yun, C.; Feng, Y. B.; Qiu, T.; Yang, J.; Li, X. Y.; Yu, L. Mechanical, Electrical, and Thermal Properties of Graphene Nanosheet/Aluminum Nitride Composites. *Ceram. Int.* **2015**, *41*, 8643−8649.

(3) Lee, C.; Wei, X. D.; Kysar, J. W.; Hone, J. Measurement of the Elastic Properties and Intrinsic Strength of Monolayer Graphene. *Science* **2008**, *321*, 385−388.

(4) Terao, R.; Tatami, J.; Meguro, T.; Komeya, K. Fracture Behavior of AlN Ceramics with Rare Earth Oxides. *J. Eur. Ceram. Soc.* **2002**, *22*, 1051−1059.

(5) Hu, G.; Chen, C. Q.; Ramesh, K. T.; McCauley, J. W. Mechanisms of Dynamic Deformation and Dynamic Failure in Aluminum Nitride. *Acta Mater.* **2012**, *60*, 3480−3490.

(6) Kim, Y. W.; Lee, S. H.; Nishimura, T.; Mitomo, M. Heat-Resistant Silicon Carbide with Aluminum Nitride and Scandium Oxide. *Acta Mater.* **2005**, *53*, 4701−4708.

(7) Kim, Y. W.; Chun, Y. S.; Nishimura, T.; Mitomo, M.; Lee, Y. H. High-Temperature Strength of Silicon Carbide Ceramics Sintered with Rare-Earth Oxide and Aluminum Nirtride. *Acta Mater.* **2007**, *55*, 727−736.

(8) Watanabe, M.; Mori, Y.; Ishikawa, T.; Lida, T.; Akiyama, K.; Sawabe, K.; Shobatake, K. X-ray Photoelectron Spectroscopy of Polycrystalline AlN Surface Exposed to the Reactive Environment of XeF_2. *Appl. Surf. Sci.* **2003**, *217*, 82−87.

(9) Jain, S. C.; Willander, M.; Narayan, J.; Overstraeten, R. V. III−nitrides: Growth, Characterization, and Properties. *J. Appl. Phys.* **2000**, *87*, 965−1006.

(10) Bartel, C. J.; Muhich, C. L.; Weimer, A. W.; Musgrave, C. B. Aluminum Nitride Hydrolysis Enabled by Hydroxyl-mediated Surface Proton Hopping. *ACS Appl. Mater. Interfaces* **2016**, *8*, 18550−18559.

(11) Weimer, A. W. *Carbide, Nitride and Boride Materials Synthesis and Processing*; Springer: Netherlands, 1997.

(12) Baranda, P. S. D.; Knudsen, A. K.; Ruh, E. Effect of Yttria on the Thermal Conductivity of Aluminum Nitride. *J. Am. Ceram. Soc.* **1994**, *77*, 1846−1850.

(13) Kocjan, A.; Krnel, K.; Kosmač, T. The Influence of Temperature and Time on the AlN Powder Hydrolysis Reaction Products. *J. Eur. Ceram. Soc.* **2008**, *28*, 1003−1008.

(14) Li, J. W.; Nakamura, M.; Shirai, T.; Matsumaru, K.; Ishizaki, C.; Ishizaki, K. Mechanism and Kinetics of Aluminum Nitride Powder Degradation in Moist Air. *J. Am. Ceram. Soc.* **2006**, *89*, 937−943.

(15) Wang, E. H.; Chen, J. H.; Hu, X. J.; Chou, K. C.; Hou, X. M. Evolution of Aluminum Hydroxides at the Initial Stage of Aluminum Nitride Powder Hydrolysis. *Ceram. Int.* **2016**, *42*, 11429−11434.

(16) Kocjan, A.; Dakskobler, A.; Kosmač, T. Superhydrophobic Nanostructured Boehmite Coatings Prepared by AlN Powder Hydrolysis. *Int. J. Appl. Ceram. Technol.* **2011**, *8*, 848−853.

(17) Bowen, P.; Highfield, J. G.; Mocellin, A.; Ring, T. A. Degradation of Aluminum Nitride Powder in an Aqueous Environmet. *J. Am. Ceram. Soc.* **1990**, *73*, 724−728.

(18) Saedi, L.; Jameh-Bozorghi, S.; Maskanati, M.; Soleymanabadi, H. The Effect of Water on the Electronic and Field Emission Properties of Inorganic AlN Nanocones: Computational Study. *Inorg. Chem. Commun.* **2018**, *90*, 86−91.

(19) Soleymani, R.; Farsi-Madan, S.; Tayeb, S.; Ghesmat-Konandeh, K. The Influence of H_2O-attaching on the NMR Parameters in the Zigzag and Armchair AlN Nanotubes: A DFT Study. *Orient. J. Chem.* **2012**, *28*, 703−714.

(20) Jindal, V.; Shahedipour-sandvik, F. Density Functional Theoretical Study of Surface Structure and Adatom Kinetics for Wurtzite AlN. *J. Appl. Phys.* **2009**, *105*, No. 084902.

(21) Ye, H. G.; Chen, G.; Zhu, Y.; Wei, S. H. Asymmetry of Adsorption of Oxygen at Wurtzite AlN (0001) and (000$\bar{1}$) Surfaces: First-principles Calculations. *Phys. Rev. B* **2008**, *73*, 44−53.

(22) Holec, D.; Mayrhofer, P. H. Surface Energies of AlN Allotropes from First Principles. *Scr. Mater.* **2012**, *67*, 760−762.

(23) Fang, Z.; Wang, E. H.; Chen, Y. F.; Hou, X. M.; Chou, K. C.; Yang, W. Y.; Chen, J. H.; Shang, M. H. Wurtzite AlN (0001) Surface Oxidation: Hints from Ab Initio Calculations. *ACS Appl. Mater. Interfaces* **2018**, *10*, 30811−30818.

(24) Payne, M. C.; Teter, M. P.; Allan, D. C.; Arias, T. A.; Joannopoulos, J. D. Iterative Minimization Techniques for Ab Initio Total-Energy Calculations: Molecular Dynamics and Conjugate Gradients. *Rev. Mod. Phys.* **1992**, *64*, 1045−1094.

(25) Perdew, J. P.; Burke, K.; Ernzerhof, M. Generalized Gradient Approximation Made Simple. *Phys. Rev. Lett.* **1996**, *77*, 3865−3868.

(26) Laasonen, K.; Sprik, M.; Parrinello, M.; Car, R. "Abinitio" Liquid Water. *J. Chem. Phys.* **1993**, *99*, 9080−9089.

(27) Lee, C.; Vanderbilt, D.; Laasonen, K.; Car, R.; Parrinello, M. Ab Initio Studies on the Structural and Dynamical Properties of Ice. *Phys. Rev. B* **1993**, *47*, 4863−4872.

(28) Tkatchenko, A. Matthias Scheffler. Accurate Molecular Van Der Waals Interactions from Ground-state Electron Density and Free-atom Reference Data. *Phys. Rev. Lett.* **2009**, *102*, No. 073005.

(29) Vanderbilt, D. Soft Self-Consistent Pseudopotentials in A Generalized Eigenvalue Formalism. *Phys. Rev. B* **1990**, *41*, 7892−7895.

(30) Ohno, T.; Shiraishi, K. First-principles Study of Sulfur Passivation of GaAs (001) Surfaces. *Phys. Rev. B* **1990**, *42*, 11194−11197.

(31) Monkhorst, H. J. Special Points for Brillouin-zone Integrations. *Phys. Rev. B* **1976**, *16*, 1748−1749.

(32) Blöchl, P. E.; Jepsen, O.; Andersen, O. K. Improved Tetrahedron Method for Brillouin-zone Integrations. *Phys. Rev. B* **1994**, *49*, 16223−16233.

(33) Wright, A. F.; Nelson, J. S. Consistent Structural Properties for AlN, GaN, and InN. *Phys. Rev. B* **1995**, *51*, 7866−7869.

(34) Hou, X. M.; Chou, K. C.; Zhong, X. C.; Seetharaman, S. Oxidation Kinetics of Aluminum Nitride at Different Oxidizing Atmosphere. *J. Alloys Compd.* **2008**, *465*, 90−96.

(35) Cao, C. W.; Feng, Y. B.; Qiu, T.; Yang, J.; Li, X. Y.; Liang, T.; Li, J. Effects of Isothermal Annealing on the Oxidation Behavior, Mechanical and Thermal Properties of AlN Ceramics. *Ceram. Int.* **2017**, *43*, 9334−9342.

DOI: 10.1021/acs.jpcc.8b11228
J. Phys. Chem. C 2019, 123, 5460−5468

(36) Böhm, M. C.; Sen, K. D.; Schmidt, P. C. Molecular Orbital Electronegativity. *Chem. Phys. Let.* **1981**, *78*, 357−360.
(37) Hu, C. L.; Chen, Y. L.; Li, J. Q. First-principles Calculations of H_2O Adsorption Reaction on the GaN (0001) Surface. *Chin. J. Struct. Chem.* **2009**, *28*, 240−244.
(38) Kocjan, A.; Dakskobler, A.; Krnel, K.; Kosmač, T. The Course of the Hydrolysis and the Reaction Kinetics of AlN Powder in Diluted Aqueous Suspensions. *J. Eur. Ceram. Soc.* **2011**, *31*, 815−823.
(39) Miao, M. S.; Weber, J. R.; Van de Walle, C. G. Oxidation and the Origin of the Two-Dimensional Electron Gas in AlGaN/GaN Heterostructures. *J. Appl. Phys.* **2010**, *107*, No. 123713.
(40) Miao, M. S.; Janotti, A.; Van de Walle, C. G. Reconstructions and Origin of Surface States on AlN Polar and Nonpolar Surfaces. *Phys. Rev. B* **2009**, *80*, No. 155319.
(41) Krukowski, S.; Kempisty, P.; Strak, P. Foundations of Ab Initio Simulations of Electric Charges and Fields at Semiconductor Surfaces within Slab Models. *J. Appl. Phys.* **2013**, *114*, No. 143705.
(42) Li, T. T.; He, C.; Zhang, W. X. Electric Field Improved the Sensitivity of CO on Substitutionally Doped Antimonene. *Appl. Surf. Sci.* **2018**, *427*, 388−395.
(43) Dong, M. M.; He, C.; Zhang, W. X. A Tunable and Sizable Bandgap of a g-C_3N_4/Graphene/ g-C_3N_4 Sandwich Heterostructure: A Van Der Waals Density Functional Study. *J. Mater. Chem. C* **2017**, *5*, 3830−3837.

DOI: 10.1021/acs.jpcc.8b11228
J. Phys. Chem. C 2019, 123, 5460−5468